Static polarizabilities and optical absorption spectra of gold clusters (Au$_n$, $n=2-14$ and 20) from first principles

Juan C. Idrobo,[1] Weronika Walkosz,[1] Shing Fan Yip,[1,*] Serdar Öğüt,[1] Jinlan Wang,[2,3] and Julius Jellinek[2]

[1]*Department of Physics, University of Illinois at Chicago, Chicago, Illinois 60607, USA*

[2]*Chemistry Division,[†] Argonne National Laboratory, Argonne, Illinois 60439, USA*

[3]*Department of Physics, Southeast University, Nanjing, 210096, People's Republic of China*

Static polarizabilities and optical absorption spectra for the ground state structures of gold clusters (Au$_n$, $n=2-14$ and 20) are investigated from first principles within static and time-dependent density functional theory. The static polarizabilities of clusters with less than 14 atoms generally increase as a function of size modulated by even-odd oscillations. The polarizabilities of Au$_{14}$ and Au$_{20}$ are noticeably lower due to the shape transition from two-dimensional to three-dimensional structures at $n=14$. The analyses of the optical absorption spectra calculated within the time-dependent local density approximation indicate that the d electrons in Au$_n$ clusters are significantly more involved in low-energy transitions and give rise to more quenched oscillator strengths (by screening the s electrons) than in Ag$_n$ clusters. These stronger effects of the d electrons in the optical properties of Au$_n$ are due to the larger degree of proximity of the s and d levels in the Au atom as compared to the Ag atom, which gives rise to stronger s-(p)-d hybridization in the molecular orbitals of Au$_n$. The calculated spectra are found to be in good agreement with experimental data and results from earlier studies for the available sizes.

PACS number(s): 78.67.−n, 36.40.Vz, 73.22.−f, 61.46.Bc

I. INTRODUCTION

Gold clusters and nanoparticles are in the center of an intense research effort fueled by the unusual degree of novelty of their physical and chemical properties and the potential this novelty holds for various technological applications.[1,2] A noble (i.e., chemically inert) metal in bulk quantities, gold exhibits truly unique, size-specific catalytic activity and selectivity at the subnanometer,[3–5] and nanometer scales.[6–8] Normally a face-centered-cubic (fcc) crystalline substance, it adopts planar conformations as the energetically most favorable structures for its clusters with about a dozen of atoms or less.[9–41] The most stable forms of many of the intermediate and larger size Au$_n$ are amorphous,[42–48] although Au$_{20}$ has been identified by a combined experimental and theoretical study[49] to possess a tetrahedrally symmetric structure, which represents a relaxed bulk fragment of the fcc lattice.[50–52] For selected sizes, gold clusters form hollow cage conformations that are energetically competitive with, or even superior to, their space-filling isomers.[53–58] The reasons for the structural peculiarities of Au$_n$ have been associated with the relativistic nature of the core electrons of Au (Refs. 15 and 57–60) and the concept of spherical aromaticity.[53–55]

Another set of features of Au$_n$, particularly relevant to nanophotonic applications, is their dielectric and optical properties. In the small and medium size range (<1 nm), these have been examined to a lesser degree. Experimentally, the optical absorption spectra of small Au clusters were obtained using a variety of techniques such as noble-gas matrix spectroscopy, resonant two-photon ionization spectroscopy, photodepletion spectroscopy, and photodissociation spectroscopy.[61–73] Theoretically, there have been few studies on the dielectric and optical properties of small and medium-sized Au clusters. Among the issues considered were the size

dependence and anisotropy of the static dipole polarizabilities[35,38,74–79] and the features of the absorption and vibronic spectra.[71,72,80–90] Most of these studies were performed within the framework of density functional theory (DFT) and time-dependent DFT (TDDFT), and some using quantum chemistry techniques such as coupled cluster and configuration interaction methods. All the theoretical explorations for the absorption spectra of Au$_n$ clusters have so far focused on a single size or a set of clusters in a narrow size range. Wang *et al.*,[82] Itkin and Zaitsevskii,[83] and Wang and Ziegler[88] computed the low-energy excitations of Au$_2$. The infrared vibronic absorption spectrum of Au$_3$ was investigated by Guo *et al.*[84] In a combined experimental and theoretical study, Schweizer *et al.* reported absorption spectra of Au$_4^+$·Ar$_n$ ($n=0-4$). For Au$_6$, Omary *et al.*[81] computed the absorption spectrum of a three-dimensional (bicapped tetrahedron of D_{2h} symmetry) isomer, while Rao *et al.*[90] investigated the spectrum of three low-lying isomers. In another combined experimental and theoretical study, absorption spectra for gold cluster anions complexed with one Xe atom, Au$_n^-$·Xe, were measured and computed for the $n=7-11$ size range. The absorption spectrum of Au$_{20}$ within TDDFT was reported by Wu *et al.*,[85] Xie *et al.*,[86] and Aikens and Schatz[87] using different exchange-correlation functionals, and by Lermé *et al.*[80] using a jellium model. Finally, Fa *et al.*[89] investigated the absorption spectra of various Au$_{32}$ isomers in the dipole approximation, where the ground and excited states were formed from the suitable Slater determinants of Kohn-Sham orbitals.

The goal of this paper is to present results on the static dipole polarizabilities and optical absorption spectra of the most stable structures of Au$_n$, $n=2-14$ and 20, as obtained within static and time-dependent density functional theory. Our optical absorption study is the first systematic application of TDDFT within the local density approximation (the

so-called TDLDA) to neutral Au_n clusters of sizes $n=1–14$ and 20 using *ab initio* pseudopotentials with explicit inclusion of the d electrons. We perform detailed comparisons of our theoretical spectra with available experimental data and obtain generally good agreement. We also compare our results with those from previous computations for the available sizes, as well as with our previous TDLDA results for Ag_n ($n=1–8$ and 11) clusters.[91–93] We show that the two main effects of the d electrons in the optical properties of noble metal clusters, namely, the quenching of the oscillator strengths and getting partially involved in low-energy excitations, are significantly enhanced in going from Ag_n to Au_n due to the stronger s-(p)-d hybridization in the latter. The rest of the paper is organized as follows. In the next section, we outline the theoretical background and the details of the computational methodologies used in this study. The results and the discussion for the static polarizabilities and optical absorption spectra are presented in Sec. III. We conclude with a brief summary in Sec. IV.

II. THEORETICAL BACKGROUND AND COMPUTATIONAL METHODS

Our computations for determining the ground state structures were performed within the framework of DFT using the Perdew-Burke-Ernzerhof (PBE) exchange-correlation functional.[94] We employed a DFT-based relativistic semicore potential,[95] fitted to all-electron relativistic results and a double numerical basis set including d-polarization functions. Full optimization of all the degrees of freedom was performed for different initial guess structures for each cluster size. Normal mode analysis was applied to every stationary configuration in order to separate the structures corresponding to minima on the potential energy surface from those that represent transition state configurations.

Our computations for the static polarizabilities and optical absorption spectra were performed in real space within the framework of the higher-order finite-difference *ab initio* pseudopotential method.[96] We used scalar-relativistic Troullier-Martins pseudopotentials[97] in nonlocal form[98] generated from the $5d^{10}6s^16p^0$ reference configuration with core radii of 2.5, 3.0, and 2.3 a.u. for s, p, and d valence electrons, respectively. The static polarizabilities were calculated within both the local density approximation (LDA) using the Ceperley-Alder (CA) exchange-correlation functional[99] and the generalized gradient approximation (GGA) using the PBE functional. The Kohn-Sham equations were solved on a three-dimensional Cartesian grid with a uniform spacing $h=0.4–0.45$ a.u. inside a large spherical domain, outside of which the wave functions were required to vanish. Spherical radii of $R_{max}=24$, 28, and 30 a.u. were used for cluster sizes of $n=1–5$, 6–14, and 20, respectively. The static polarizabilities were computed using a finite-field method[100,101] with an external electric field magnitude of 10^{-3} a.u. The optical absorption spectra were calculated using adiabatic TDLDA within the frequency domain formalism of Casida.[102] In this formalism, the energies Ω_i and the oscillator strengths f_i of the electronic system are the poles and residues of the dynamical polarizability, $\alpha(\omega)=\Sigma_i f_i/(\Omega_i^2-\omega^2)$. Ω_i and f_i are

calculated by diagonalizing the full TDLDA matrix.[103] We tested the convergence of the optical spectra up to 6 eV with respect to R_{max} and the total number of single-particle (Kohn-Sham) orbitals. The resulting number of grid points (Hamiltonian size N) and TDLDA matrix sizes M (determined by the number of occupied and unoccupied orbital pairs) ranged from $N \sim 900\,000$ to $1\,800\,000$, and $M \sim 2,100$ (Au atom) to 12 100 (Au_{20}). Since Au_n clusters with an odd number of atoms have an odd number of valence electrons, they call for a spin-polarized treatment. Our tests for Au, Au_3, and Au_5 have revealed that the restricted (spin-unpolarized) treatment gives rather accurate excitation energies and oscillator strengths. The largest deviation of 0.13 eV is observed in the $6s \rightarrow 6p$ excitation energy of the Au atom. For larger clusters, the differences between spin-polarized and restricted treatments are less than 0.02 eV. Therefore, the bulk of the TDLDA computations were performed using the restricted formalism.

III. RESULTS AND DISCUSSION

A. Structures

As mentioned in the Introduction, the structures of small and medium size gold clusters have been the subject of a number of computational studies and they are discussed in the literature extensively.[9–59] Although different computational approaches yield somewhat different results, particularly regarding the details, a dominant common finding is the persistence of planar structures as the energetically most favorable conformations of Au_n with n about a dozen of atoms or less. This finding is supported by mobility measurements of charged gold clusters,[18,19] and it is born out by our computations as well.[54]

The most stable isomeric forms of Au_n, $n=2–14$ and 20, as obtained within our DFT/PBE treatment described in Sec. II, are displayed in Fig. 1. The figure also shows the symmetries and the bond lengths of these energetically preferred conformations. Except for Au_{14} and Au_{20}, they are planar. Their binding energy per atom (Table I) increases almost monotonically with size, but remains substantially below the cohesive energy of bulk gold (3.81 eV). Their computed electron affinities are listed together with those measured for Au_n, $n=2–14$ and 20, in Table I. The two sets of values exhibit a good agreement. Below, we present and analyze the static dipole polarizabilities and optical absorption spectra as obtained within our computations for the isomers of Au_n, $n=2–14$ and 20, displayed in Fig. 1.

B. Static polarizabilities

The average static polarizabilities, $\langle\alpha\rangle=(\alpha_{xx}+\alpha_{yy}+\alpha_{zz})/3$, of Au_n computed with the CA and PBE functionals are shown in Fig. 2. For the Au atom, the CA and PBE values are 5.08 and 5.21 Å^3, respectively. These are in reasonable agreement with the reported experimental estimates of 4.46 ± 0.59 Å^3 (Ref. 2) and 5.79 ± 1.45 Å^3 (Ref. 77). They are also within <20% of the values of 4.13 Å^3 (Ref. 77) and 5.34 Å^3 (Ref. 74), obtained by using different quantum chemistry methods. Recently, using the SIESTA code with
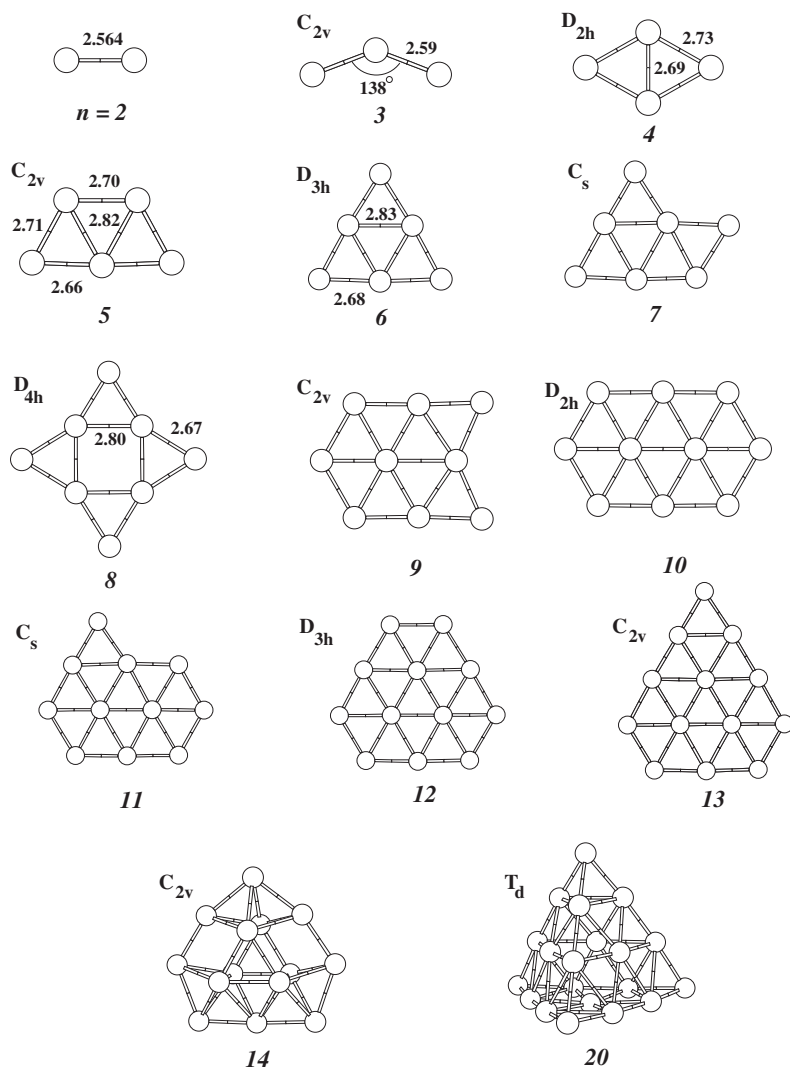
FIG. 1. Calculated ground state geometries of Au$_n$, $n=2-14$ and 20. The symmetries of the clusters, some of the bond lengths (in Å), and one bond angle are also displayed.

pseudopotential parameters similar to ours, Fernández *et al.* have reported a value of 3.04 Å^3 for the Au atom polarizability.[35] The reason behind the significant difference of this value from ours and the experimental estimates is not clear. We note that our CA and PBE polarizabilities of the Au atom are ~20% smaller than those of the Ag atom[91] due to enhanced screening of the s electrons by the d electrons (core polarization) in the former, which also manifests itself in the optical properties.

The computed polarizabilities per atom for $n \lesssim 13$ exhibit even-odd oscillations characteristic of clusters of atoms with an odd number of electrons. Overall, $\langle \alpha \rangle$ increases as a function of n, modulated by these oscillations, up to $n=13$. The diagonal z component α_{zz} (where z is the direction perpendicular to the plane of the clusters), on the other hand, decreases smoothly in this size range. This has been attributed[76] to a decreasing number of undercoordinated Au atoms as the size of the cluster increases. The shape transition at $n=14$ from planar to compact three-dimensional structures is reflected by a significant decrease in the polarizability of Au$_{14}$. This decrease is in accord with the expectation that the polarizability per atom of a cluster is a quantity related to its volume per atom, which decreases as the

cluster becomes more compact.[91,100,104] In addition to the finite-field method, the static polarizabilities can also be calculated from TDLDA excitation energies Ω_i and oscillator strengths f_i as $\alpha(0)=\Sigma_i f_i/\Omega_i^2$, where the sum is over all excitations. For sp-bonded clusters, such as those of Na and Si, restricting this sum to those excitations for which $\Omega_i < 10$ eV is typically enough for TDLDA static polarizabilities to converge to within a few percent of the values obtained from the finite-field method.[100] However, in noble metal clusters the effect of d-electron screening and the resulting quenching of the oscillator strengths make this convergence rather slow.[91,92] As shown in Fig. 2, the TDLDA static polarizabilities are approximately 10% below the corresponding finite-field values, in spite of including excitations with $\Omega_i \lesssim 13$ eV.

Figure 2 also shows the polarizabilities computed by different groups for the same ground state structures. Overall, the general increasing trend of $\langle \alpha \rangle$ as a function of size modulated by even-odd oscillations is also observed in the computations of Fernández *et al.*[35] and Li *et al.*,[38] while the values of Zhao *et al.*[76] are significantly smaller than ours and show a rather monotonic increase with size. On average, our PBE values are approximately 22% larger than those of

TABLE I. The binding energies (BEs) and electron affinities (EAs) computed for the most stable conformations of gold clusters shown in Fig. 1 using the DFT/PBE approach and the measured EA for Au_n, $n=2-14$ and 20.

Cluster	BE (eV)	Computed EA[a] (eV)	Measured EA[b] (eV)
Au_2	1.07	1.82	1.92
Au_3	1.11	3.51	3.88
Au_4	1.42	2.68	2.70
Au_5	1.55	3.01	3.06
Au_6	1.77	2.09	2.06
Au_7	1.72	3.32	3.40
Au_8	1.84	2.80	2.73
Au_9	1.81	3.65	3.81
Au_{10}	1.91	3.07	3.89
Au_{11}	1.90	3.70	3.76
Au_{12}	1.97	3.21	3.03
Au_{13}	1.95	3.88	3.91
Au_{14}	2.02	3.29	2.94
Au_{20}	2.17	2.65	2.75

[a]Reference 54.
[b]References 20 and 49.

Fernández *et al.*, and they are in very good agreement (only 3% higher on average) than the most recent results from Li *et al.* For Au_2, our longitudinal ($\alpha_\parallel$) and transverse ($\alpha_\perp$) GGA polarizability per atom values of $\alpha_\parallel = 8.46$ Å^3 and $\alpha_\perp = 4.42$ Å^3 are also in good agreement with the four-component relativistic Dirac-Coulomb Hartree-Fock level computations of Saue and Jensen,[75] who reported the values of 8.46 and 4.87 Å^3, respectively.

C. Optical absorption spectra

The optical absorption spectra of Au_n, $n=2-14$ and 20, are plotted in Fig. 3. Experimental optical absorption spectra for neutral Au_n clusters (in gas phase or embedded in Ar
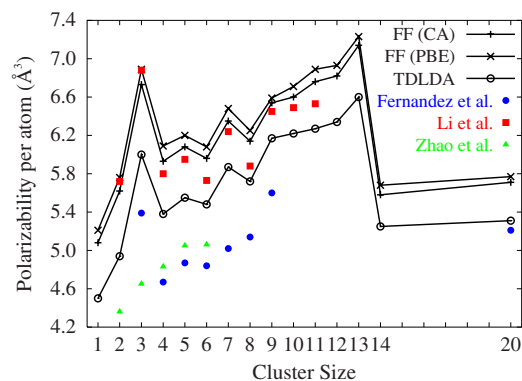

FIG. 2. (Color online) Static dipole polarizabilities of Au_n computed with the finite-field (FF) method using the CA and PBE exchange-correlation functionals and from the TDLDA excitation energies and oscillator strengths as a function of n. Also shown are the results from previous studies by Fernández *et al.* (Ref. 35), Li *et al.* (Ref. 38), and Zhao *et al.* (Ref. 76).
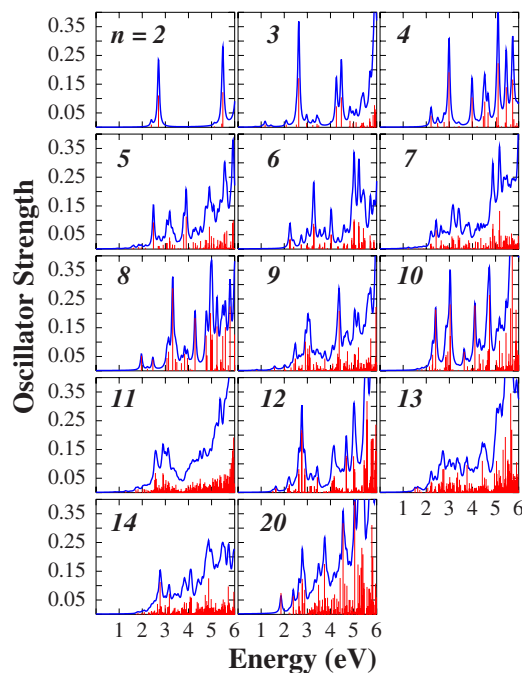

FIG. 3. (Color online) The TDLDA excitation energies and the corresponding oscillator strengths for Au_n, $n=2-14$ and 20. The spectra were broadened using Lorentzians of half-width 0.05 eV.

matrices) are available for $n=1-3$. The experimental values, our computed TDLDA transitions assigned to them, and the results of other theoretical treatments for this size range are summarized in Table II. For the Au atom, the calculated $6s \rightarrow 6p$ excitation energy is 5.22 eV. Neglecting the spin polarization results in an excitation energy of 5.35 eV. The oscillator strength (OS) for this transition is $f=0.31$, which is half the OS of the $5s \rightarrow 5p$ transition we computed for the Ag atom.[91] This reduction is due to increased screening of the s electrons by the d electrons in Au compared to Ag. The agreement with existing TDLDA computations,[105,106] which give a value of 5.23 eV, is excellent. The measured values for the $6s \rightarrow 6p_j$ transitions are 4.64 and 5.11 eV for $j=1/2$ and $j=3/2$ spin-orbit split levels, respectively.[107] Since our scalar relativistic computations take into account relativistic corrections in an average sense, our computed value of 5.22 eV should be compared with the weighted average of the two experimental transitions, which is 4.95 eV. The agreement within $\sim5\%$ between experiment and TDLDA computations is fairly good. The next strong TDLDA transition occurs at 7.06 eV with an OS of $f=0.43$. This corresponds to $6s \rightarrow 7p_j$ transition, experimentally measured at 7.44 and 7.53 eV for $j=1/2$ and $j=3/2$, respectively. Our computed value underestimates the experimental average of 7.5 eV by $\sim6\%$.

For Au_2, our computed TDLDA transitions with nonvanishing OS below 6.5 eV are at 2.39 eV ($f=0.01$), 2.70 eV ($f=0.11$), 5.12 eV ($f=0.003$), 5.43 eV ($f=0.013$), 5.49 eV ($f=0.12$), 6.14 eV ($f=0.31$). We have associated the so-called $X \rightarrow A$ transition measured experimentally[61,65] at 2.44 eV with our computed value at 2.39 eV. The $X \rightarrow B$ transition measured experimentally[61,65] at 3.18 eV corre-

TABLE II. Comparison of experimental absorption energies, our computed TDLDA values and oscillator strengths (OS), and results from other theoretical treatments. Values in parentheses denote the lower and upper bounds for a range of closely-spaced transitions. All energies are in eV.

Cluster	Expt.	TDLDA energy	OS	Other theory
Au	4.95[a]	5.22	0.31	5.23[b]
Au$_2$				
$X \rightarrow A$	2.44,[c] (2.44–2.49)[d]	2.39	0.01	2.47,[e] 2.79[f]
$X \rightarrow B$	3.18[c,d]	2.70	0.11	2.94,[f] 3.30[e]
$X \rightarrow C$	3.85,[g] 3.91[h]	3.70	0.00	3.20[f]
$X \rightarrow D$	5.95[h]	5.49	0.06	5.50[f]
$X \rightarrow E$	6.26[h]	6.14	0.15	5.80[f]
Au$_3$	2.63,[g,h] 2.43–2.71[i]	2.63	0.17	
	3.35[i]	(3.42–3.49)	0.02	
	4.11[i]	4.24	0.08	
	4.35[i]	4.47	0.10	
	4.81[i]	(4.81–4.87)	0.03	
	5.37[i]	(5.35–5.45)	0.06	

[a]This is the weighted average of actual experimental values of 4.64 and 5.11 eV in Ref. 107.
[b]References 105 and 106
[c]Reference 65.
[d]Reference 61.
[e]Reference 83.
[f]Reference 82.
[g]Reference 64.
[h]Reference 63.
[i]Reference 68.

TABLE III. TDLDA absorption energies (in eV) and the corresponding oscillator strengths (in parentheses) for Au$_n$ ($n=4$–9) clusters. The transitions with energies $\Omega \lesssim 5.5$ eV and oscillator strengths $f \geq 0.01$ are shown. Some transitions within 0.01 eV of each other are shown as a single transition with the combined oscillator strength. The transitions with $f \geq 0.1$ are given in bold.

Cluster	TDLDA energies (oscillator strengths)
Au$_4$	2.21 (0.04), 2.49 (0.02), 2.77 (0.02), **2.98 (0.19)**, **3.98 (0.10)**, 4.47 (0.04), 4.53 (0.09), 4.67 (0.05), 5.04 (0.03), **5.11 (0.22)**, 5.42 (0.02), **5.46 (0.14)**
Au$_5$	2.48 (0.09), 2.69 (0.01), 2.73 (0.01), 2.90 (0.02), 3.07 (0.04), 3.19 (0.07), 3.31 (0.02), 3.40 (0.02), 3.79 (0.05), **3.90 (0.11)**, 4.21 (0.02), 4.30 (0.02), 4.38 (0.01), 4.52 (0.03), 4.72 (0.04), 4.78 (0.03), 4.84 (0.02), 4.91 (0.09), 4.99 (0.05), 5.09 (0.05) 5.27 (0.03), 5.36 (0.05), 5.41 (0.03), 5.46 (0.02)
Au$_6$	2.24 (0.03), 2.26 (0.04), 2.73 (0.03), 2.98 (0.03), 3.24 (0.01), 3.27 (0.09), 3.29 (0.08), 3.54 (0.03), 3.75 (0.04), **4.03 (0.10)**, 4.59 (0.04), 4.70 (0.01), 4.74 (0.02), 4.91 (0.03), 4.93 (0.04), 4.96 (0.02)
Au$_7$	2.18 (0.02), 2.21 (0.02), 2.43 (0.07), 2.63 (0.01), 2.65 (0.03), 2.76 (0.03), 2.82 (0.01), 2.89 (0.01), 2.93 (0.01), 3.11 (0.04), 3.15 (0.04), 3.17 (0.02), 3.19 (0.03), 3.25 (0.02), 3.38 (0.05), 3.41 (0.03), 3.45 (0.04), 3.61 (0.01), 3.67 (0.01), 3.71 (0.02), 3.75 (0.02), 3.83 (0.03), 3.88 (0.02), 4.13 (0.03), 4.23 (0.05), 4.36 (0.04), 4.47 (0.01), 4.49 (0.01), 4.58 (0.02), 4.69 (0.01), 4.77 (0.04), 4.79 (0.03), **4.87 (0.19)**, 4.96 (0.05), 5.03 (0.03), 5.07 (0.02) 5.15 (0.07), **5.17 (0.15)**
Au$_8$	1.96 (0.05), 2.46 (0.04), 3.07 (0.05), 3.14 (0.07), **3.32 (0.29)**, 3.44 (0.04), 3.49 (0.03), 3.69 (0.03), 3.83 (0.06), 3.95 (0.05), **4.29 (0.18)**, **4.77 (0.12)**, 4.80 (0.05), **4.96 (0.20)**, **5.02 (0.23)**, **5.24 (0.17)**, **5.41 (0.13)**, **5.48 (0.12)**
Au$_9$	1.58 (0.01), 2.01 (0.01), 2.29 (0.01), 2.42 (0.03), 2.48 (0.08), 2.63 (0.03), 2.74 (0.01), 2.77 (0.02), **2.92 (0.10)**, **3.02 (0.10)**, 3.02 (0.06), **3.11 (0.13)**, 3.27 (0.03), 3.39 (0.03), 3.44 (0.02), 3.56 (0.02), 3.58 (0.01), 3.76 (0.04), 4.10 (0.04), 4.23 (0.01), 4.27 (0.03), 4.31 (0.06), 4.34 (0.05), **4.38 (0.21)**, 4.43 (0.04), 4.57 (0.02), 4.59 (0.05), 4.66 (0.02), 4.68 (0.04), 4.74 (0.07), 4.81 (0.02), 4.91 (0.03), 5.03 (0.08), 5.05 (0.06), 5.08 (0.06)

sponds to our computed transition at 2.70 eV. The $X \rightarrow C$ transition measured at 3.85 eV (Ref. 64) and 3.91 eV (Ref. 63) is observed only for matrix-deposited Au$_2$ clusters. Similar to the suggestion by Wang *et al.*,[82] we assign our computed transition at 3.70 eV with a vanishing oscillator strength with the $X \rightarrow C$ transition. We speculate that it is the coupling of the cluster to the matrix that makes this otherwise dipole-forbidden transition appear as an optical transition with a low oscillator strength, which is consistent with the fact that it is not observed in gas-phase measurements.[61,65] We assign the rest of the measured transitions $X \rightarrow D$ (5.95 eV) (Ref. 63) and $X \rightarrow E$ (6.26 eV) (Ref. 63) with our computed doubly degenerate transitions at 5.49 and 6.14 eV, respectively.

Our spin-polarized TDLDA spectrum for Au$_3$ consists of several peaks in the low-energy range (<5.5 eV) for which experimental data are currently available. The most prominent peak occurs at 2.63 eV with an OS of $f=0.17$. We associate this strong transition with the experimentally measured line at 2.63 eV by Klotzbücher and Ozin[63] and later confirmed by Marcus and Schwentner.[64] The measurements of Fedrigo *et al.*, on the other hand, find two intense lines at 2.43 and 2.71 eV in this energy range.[68] While the line at 2.71 eV could perhaps be associated with the 2.63 eV transition found in earlier experiments and our present computa-

tions, the origin of the 2.43 eV transition is not clear. The rest of the absorption lines measured by Fedrigo *et al.* at 3.35, 4.11, 4.35, 4.81, and 5.37 eV can be accounted for by our computed transitions at 3.42–3.49 eV (a series of closely spaced transitions in this energy range with a total OS of $f=0.02$), 4.24 eV ($f=0.075$), 4.47 eV ($f=0.1$), 4.81–4.87 eV ($f=0.025$), and 5.35–5.45 eV ($f=0.06$), respectively. In addition to these, our computations yield a few more peaks at 2.97 eV ($f=0.015$), 4.97 eV ($f=0.014$), and 5.11 eV ($f=0.018$), which have not been observed in the available ex-

TABLE IV. TDLDA absorption energies (in eV) and the corresponding oscillator strengths (in parentheses) for Au_n ($n=10-13$) clusters. The transitions with energies $\Omega \lesssim 5$ eV and oscillator strengths $f \geq 0.02$ are shown. Some transitions within 0.01 eV of each other are shown as a single transition with the combined oscillator strength. The transitions with $f \geq 0.1$ are given in bold.

Cluster	TDLDA energies (oscillator strengths)
Au_{10}	2.14 (0.02), 2.27 (0.08), **2.41 (0.21)**, 2.84 (0.05), 2.86 (0.06), 2.93 (0.07), 2.97 (0.02), **3.04 (0.35)**, 3.64 (0.07), 3.79 (0.02), **4.10 (0.23)**, 4.29 (0.06), 4.34 (0.03), 4.45 (0.04), 4.58 (0.03), 4.60 (0.02), 4.61 (0.02), 4.64 (0.04), **4.66 (0.10)**, 4.70 (0.08), **4.74 (0.26)**
Au_{11}	2.54 (0.04), 2.57 (0.07), 2.61 (0.05), 2.65 (0.03), 2.67 (0.02), 2.72 (0.03), 2.76 (0.02), 2.84 (0.02), 2.88 (0.09), 2.99 (0.05), 3.04 (0.06), 3.09 (0.02), 3.11 (0.05), 3.13 (0.04), 3.17 (0.05), 3.30 (0.02), 3.36 (0.02), 3.37 (0.02), 3.39 (0.02), 3.45 (0.03), 3.88 (0.02), 3.92 (0.02), 3.99 (0.04), 4.07 (0.02), 4.08 (0.03), 4.15 (0.02), 4.19 (0.04), 4.23 (0.02), 4.28 (0.04), 4.35 (0.03), 4.38 (0.03), 4.44 (0.02), 4.49 (0.03), 4.51 (0.05), 4.53 (0.02), 4.61 (0.02), 4.64 (0.02), 4.65 (0.03), 4.67 (0.03), 4.71 (0.04), 4.75 (0.02), 4.78 (0.02), 4.82 (0.02), 4.87 (0.02), 4.91 (0.03), 4.93 (0.03)
Au_{12}	1.63 (0.03), 2.16 (0.03), 2.21 (0.05), 2.49 (0.02), **2.63 (0.15)**, **2.76 (0.42)**, **2.89 (0.15)**, 3.12 (0.04), 3.18 (0.04), 3.31 (0.04), 3.38 (0.02), **3.43 (0.10)**, 4.07 (0.07), 4.12 (0.08), **4.17 (0.14)**, 4.25 (0.04), 4.31 (0.03), 4.39 (0.03), 4.52 (0.03), **4.68 (0.25)**, 4.76 (0.03), **5.00 (0.23)**
Au_{13}	1.51 (0.02), 1.63 (0.02), 2.07 (0.02), 2.19 (0.02), 2.21 (0.04), 2.24 (0.03), 2.39 (0.02), 2.55 (0.06), 2.57 (0.03), 2.59 (0.02), 2.65 (0.05), 2.69 (0.04), 2.71 (0.08), 2.76 (0.08), 2.87 (0.02), 2.89 (0.05), 2.96 (0.05), 3.00 (0.07), 3.04 (0.04), 3.13 (0.06), 3.16 (0.02), 3.19 (0.7), 3.32 (0.07), 3.36 (0.07), 3.41 (0.02), 3.43 (0.04), 3.45 (0.02), 3.49 (0.03), 3.66 (0.04), 3.69 (0.03), **3.76 (0.10)**, 3.87 (0.03), 3.96 (0.03), 4.00 (0.02), 4.09 (0.04), 4.12 (0.02), 4.16 (0.03), 4.26 (0.02), 4.29 (0.03), 4.33 (0.02), 4.35 (0.02), 4.39 (0.02), 4.44 (0.02), 4.50 (0.05), 4.52 (0.08), 4.56 (0.03), 4.59 (0.05), 4.61 (0.02), 4.67 (0.04), 4.95 (0.07), 4.98 (0.03), 4.99 (0.04)

periments, most likely due to relatively small oscillator strengths.

For the rest of the clusters ($n=4-14$ and 20), the computed low-energy transitions (up to $5-5.5$ eV) and the corresponding oscillator strengths are displayed in Tables III–V. Typically, clusters with an even number of atoms (valence electrons) exhibit sharper peaks than those with an odd number of electrons, which exhibit densely spaced peaks of low

OS. In this size range, photodepletion spectra for Au_nXe_m are available[70] for $n=7$, 9, 11, 13 and $m=1,2$. The general trends observed in these measurements are (i) a local absorption maximum at ~ 2.9 eV, (ii) a local minimum in the absorption at ~ 4.3 eV, and (iii) a rising absorption above 4.6 eV. These general features, in particular, the local maximum around 2.9 eV, are accounted for to some extent in our computations, but there are discrepancies as well, e.g., for $n=9$, we observe a local maximum at 4.3 eV rather than a minimum. We note that is it not straightforward to identify the absorption peaks from the available photodepletion spectra for a meaningful comparison with our computed transitions. The main reason for this is the low density of energies at which measurements were made, which makes it difficult to determine if the measured absorption corresponds to the maximum of the peak.

In a more recent study, Zheng *et al.*[73] measured the absorption and emission lines from highly fluorescent, water-soluble Au nanoclusters of sizes $n=5$, 8, 13, 23, and 31. The measured excitation energies for Au_5, Au_8, and Au_{13} are 3.76, 3.22, and 2.86 eV, respectively, which are in very good agreement with our computations. For Au_5, our computed transition with the largest oscillator strength of $f=0.10$ is at 3.90 eV, which is also close to another relatively strong transition at 3.79 eV with $f=0.05$ (Table III and Fig. 3). For Au_8, again our computed transition with the largest oscillator strength of $f=0.29$ occurs at 3.32 eV, which is only 0.1 eV higher than the experimentally measured value. For Au_{13}, our two computed transitions at 2.71 and 2.76 eV with relatively large oscillator strengths of $f=0.08$ each (Table IV) give rise to a local maximum in our theoretical absorption spectrum at 2.74 eV (see Fig. 3), which is within ~ 0.1 eV of the experimental value.

While there are no experimental data available for the absorption spectrum of the tetrahedral Au_{20} cluster, several groups have recently reported its computed spectrum within TDDFT.[85–87] The results from existing computations are shown for comparison with each other in Fig. 4. Overall, our computed values are in good agreement with those of Aikens and Schatz,[87] other than a 0.1–0.2 eV energy shift, which is due to the different exchange-correlation functionals (GGA-BP86 versus LDA-CA) used in TDDFT computations. In the 1.9–3.0 eV range, Xie *et al.*[86] find the onset of absorption to be around 1.93 eV followed by the first significant peak at 2.74 eV, which are in good agreement with our corresponding values of 1.86 and 2.78 eV (Table V). The computations of Wu *et al.*,[85] on the other hand, seem to give excitation energies which are shifted to the blue by $\sim 0.4-0.5$ eV with respect to our values. The LB94 exchange-correlation functional used in the computations of Wu *et al.* is the most likely reason for this somewhat significant difference. If this shift is taken into account, our analysis of the *site* character of the low-energy transitions seems to be in good agreement with those of Wu *et al.* To show this, let us first define $\Lambda_i(\mathbf{r})$ for a given transition of index i as $\Lambda_i(\mathbf{r}) = \Sigma_{vc} |F_i^{vc}|^2 |\phi_v(\mathbf{r})|^2$, where the double index vc labels the entries of the TDLDA eigenvector F_i, which is composed of occupied-unoccupied (or "valence-conduction") Kohn-Sham orbital pairs. These entries are normalized to unity as $\Sigma_{vc} |F_i^{vc}|^2 = 1$ and $\phi_v(\mathbf{r})$ denotes the corresponding occupied Kohn-Sham orbital. If we

TABLE V. TDLDA absorption energies (in eV) and the corresponding oscillator strengths (in parentheses) for Au_n ($n = 14, 20$) clusters. The transitions with energies $\Omega \lesssim 5.5$ eV and oscillator strengths $f \geq 0.02$ are shown. Some transitions within 0.01 eV of each other are shown as a single transition with the combined oscillator strength. The transitions with $f \geq 0.1$ are given in bold.

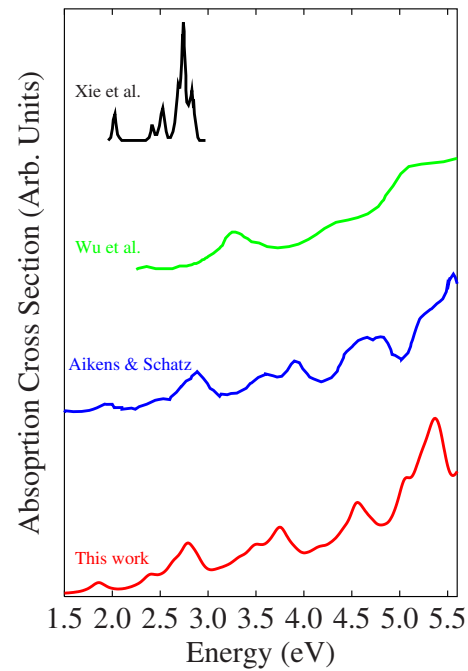| Cluster	TDLDA energies (oscillator strengths)
Au_{14}	2.66 (0.04), 2.73 (0.02), 2.75 (0.02), **2.77 (0.11)**, 2.80 (0.03), 2.84 (0.04), 2.99 (0.03), 3.09 (0.02), 3.14 (0.03), 3.18 (0.07), 3.38 (0.02), 3.42 (0.02), 3.55 (0.03), 3.71 (0.02), 3.74 (0.05), 3.78 (0.02), 3.82 (0.08), 3.85 (0.02), 3.88 (0.02), 3.91 (0.04), 4.05 (0.03), 4.07 (0.06), 4.11 (0.06), 4.13 (0.06), 4.33 (0.02), 4.38 (0.04), 4.42 (0.05), 4.44 (0.02), 4.50 (0.04), 4.60 (0.03), 4.62 (0.02), 4.68 (0.02), 4.72 (0.02), 4.73 (0.07), 4.76 (0.02), 4.78 (0.03), 4.79 (0.05), 4.82 (0.06), 4.85 (0.02), **4.87 (0.13)**, 4.89 (0.03), 4.94 (0.05), 4.98 (0.07), 4.99 (0.04)
Au_{20}	1.86 (0.08), 2.39 (0.09), 2.63 (0.08), **2.78 (0.23)**, 2.85 (0.04), 2.89 (0.09), 3.08 (0.02), 3.19 (0.02), 3.31 (0.04), 3.35 (0.04), 3.41 (0.03), 3.46 (0.03), **3.48 (0.10)**, 3.54 (0.05), 3.62 (0.03), 3.66 (0.05), **3.74 (0.18)**, 3.76 (0.02), 3.79 (0.06), 3.80 (0.03), 3.87 (0.06), 3.93 (0.05), 4.04 (0.05), 4.12 (0.06), 4.18 (0.07), 4.22 (0.02), 4.28 (0.06), 4.31 (0.03), 4.35 (0.05), **4.42 (0.13)**, 4.50 (0.02), **4.54 (0.32)**, 4.60 (0.02), **4.62 (0.11)**, 4.66 (0.02), **4.71 (0.13)**, 4.81 (0.05), 4.85 (0.05), 4.94 (0.05), 4.96 (0.05), **5.05 (0.39)**, 5.15 (0.05), **5.19 (0.18)**, 5.21 (0.08), 5.24 (0.03), **5.26 (0.16)**, **5.32 (0.20)**, **5.36 (0.26)**, 5.38 (0.06), **5.40 (0.23)**, 5.42 (0.06), **5.45 (0.17)**

FIG. 4. (Color online) Comparison of our TDLDA spectrum for Au_{20} with spectra from previous studies by Aikens and Schatz (Ref. 87), Wu et al. (Ref. 85), and Xie et al. (Ref. 86).

91) with $E_c = 6$ eV. We first note that in the common size range, the integrated oscillator strengths (IOSs) for Au_n clusters are considerably lower (by $\sim$40%) than those for Ag_n. The reason for this is the increased screening of the s electrons by the d electrons in Au_n compared to Ag_n. This screening is well known to quench the oscillator strengths in noble metal clusters[91–93] in comparison to those of alkali metals, for which the oscillator strengths per s electron inte-

weight each transition in a given energy range from E_1 to E_2 with its oscillator strength f_i and sum over all the transitions in the given range, we can obtain an effective "optical charge density" $\Lambda_{E_1-E_2}(\mathbf{r}) = \Sigma_{E_1 < \Omega_i < E_2} f_i \Lambda_i(\mathbf{r})$, which allows us to map the charge density associated with transitions in the E_1 to E_2 energy range (or with a single transition).[108] We have analyzed the spatial distribution of some of the main peaks in the spectrum of Au_{20} via volumetric plots of $\Lambda(\mathbf{r})$. For example, as shown in Fig. 5(a), the first significant peak at 1.86 eV involves excitations from the face-centered atoms of the tetrahedron in agreement with the assignment of Wu et al. for their lowest-energy peak at 2.35 eV. Next, as shown in Fig. 5(b), the two (almost degenerate) transitions at 2.777 and 2.785 eV are excitations originating mainly from the edge atoms with some admixture from the face-centered ones, in agreement with the assignment of Wu et al. for their computed transitions at 3.20 and 3.32 eV. The excitations originating from the four vertex atoms, on the other hand, mainly occur in the 3–4 eV energy range (in particular, at 3.48 and 3.74 eV), as shown in Fig. 5(c).

The results for the oscillator strengths of Au_n are shown in Fig. 6, which displays the computed oscillator strengths per s electron integrated up to cutoff energies of $E_c = 3, 4, 5,$ and 6 eV along with the same results for Ag_n ($n \leq 8$) (Ref.
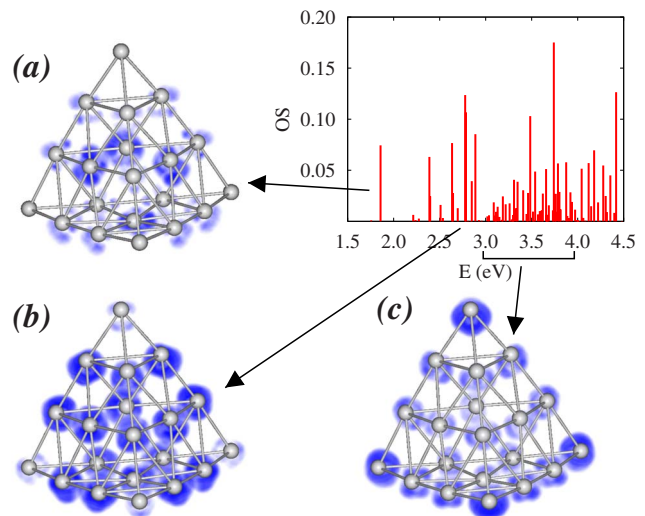

FIG. 5. (Color online) Volumetric density plots of the "optical charge densities" $\Lambda(\mathbf{r})$ of Au_{20} for (a) the excitation at 1.86 eV, (b) the excitations at 2.777 and 2.785 eV combined, and (c) the excitations in the 3–4 eV energy range. The darker gray (blue) areas show where $\Lambda(\mathbf{r})$ has higher values.
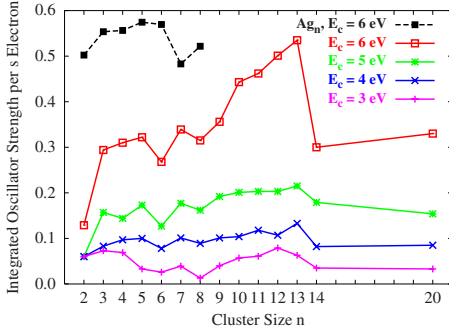
FIG. 6. (Color online) The oscillator strengths per *s* electron of the Au$_n$ clusters (solid lines) integrated up to cutoff energies of $E_c = 3-6$ eV as a function of the cluster size. Also shown (dashed lines) are the same results for Ag$_n$ ($n \leq 8$) at $E_c = 6$ eV (Ref. 91).

grated up to ~6 eV is close to 1. Second, we observe that Au$_n$ clusters, in particular, for $8 < n < 14$, have significantly large absorption cross sections in the 5–6 eV energy range (see Fig. 3), which is reflected in Fig. 6 by the sudden increase of the IOS in going from $E_c = 5-6$ eV. This large increase makes the noticeable drop at $n = 14$ more obvious, as the IOS values for Au$_{14}$ and Au$_{20}$ are ~40% lower than that of Au$_{13}$. Increasing E_c up to 10 eV does not change this behavior. The observed trend in the IOS as a function of size is due to the underlying atomic structure, similar to the trend observed in the static dipole polarizabilities (see Fig. 2). Namely, it is the change from two-dimensional to three-dimensional structures at $n = 14$ for Au$_n$ clusters that is responsible for the observed drop in the IOS. In Fig. 6, the same trend is observed for Ag$_n$ clusters at $n = 7$, which is the size at which the structural change occurs for Ag$_n$.[91] As mentioned earlier, the static polarizability can be calculated from TDLDA spectra using $\alpha(0) = \Sigma_i f_i / \Omega_i^2$. While restricting the summation over all the transitions to those below a certain cutoff energy E_c lowers the polarizability values (compared to those calculated from the finite-field method), the trend as a function of size typically remains the same even with E_c's as low as 6 eV. The polarizability computed this way is closely related to the oscillator strengths integrated up to a cutoff energy E_c which can be written as IOS($< E_c$) $= \Sigma_{i,\Omega_i < E_c} f_i$. If we now approximate $\alpha(0)$ using an average transition energy $\bar{\Omega}$ as

$$\alpha(0) \approx \sum_{i,\Omega_i < 6 \text{ eV}} \frac{f_i}{\Omega_i^2} \approx \frac{1}{\bar{\Omega}^2} \sum_{i,\Omega_i < 6 \text{ eV}} f_i = \frac{\text{IOS}(< 6 \text{ eV})}{\bar{\Omega}^2}, \tag{1}$$

we obtain an almost *size-independent* value for $\bar{\Omega}$ $= 4.09 \pm 0.08$ eV over the size range $n = 4-14$ and 20.

In our previous study on small Ag$_n$ ($n \leq 8$) clusters,[91] we identified the two roles played by the *d* electrons in the optical spectra as (i) quenching of the oscillator strength (OS) by screening the *s* electrons, and (ii) getting partially involved in low-energy excitations. As discussed above (see Fig. 6), the screening effect is significantly enhanced in Au$_n$ clusters compared to Ag$_n$ clusters. Similarly, we can expect

that the degree of the involvement of the *d* electrons in low-energy excitations of Au$_n$ will also increase. This can already be inferred from the electronic structure of the two elements at the atomic level by considering the difference in the separation of the *s* and *d* energy levels. From the Kohn-Sham energies, we find that the 5*d*-6*s* separation in Au is ~2 eV smaller compared to the 4*d*-5*s* separation in Ag. This suggests that the *s*-*d* hybridization will play an important role in the electronic and optical properties of Au$_n$. For example, in Ag$_2$, because of the large *s*-*d* atomic separation, the atomic *d* orbitals hybridize among themselves, almost completely decoupled from the *s* orbitals. As such, the first ten doubly occupied (due to spin degeneracy) levels in Ag$_2$ have purely *d* character. The highest occupied molecular orbital (HOMO) is a bonding combination of 5*s* atomic orbitals, and the lowest unoccupied molecular orbital (LUMO) is an antibonding combination. In Au$_2$, on the other hand, the *s*-(*p*)-*d* hybridization results mostly in occupied Kohn-Sham orbitals of mixed *s*-*d* character with a small *p* admixture. For example, within LDA using the CA functional the HOMO and the doubly degenerate HOMO-1 have large *d* characters (80% and 85%, respectively), while the level with the largest *s* character of 85% (the bonding combination of 6*s* electrons) is HOMO-2. This mixing naturally affects the orbital characters of the optical transitions. Using the same analysis by identifying the few dominant *vc* pairs appearing in the TDLDA eigenvector of a given transition, as described in Ref. 91, we have examined the orbital characters of the optical excitations in Au$_n$ clusters. The example shown in Fig. 7 for some of the low-energy transitions in Au$_2$ highlights the differences between Au$_2$ and Ag$_2$. We find that the computed lowest-energy transition at 2.39 eV (associated with the experimental $X \rightarrow A$ line), almost purely involves (with 99.5% weight in the corresponding eigenvector) the HOMO-1/LUMO *vc* pair. Given that HOMO-1 in Au$_2$ has 85% *d* character, we immediately see that the lowest allowed optical transition in Au$_2$ is mostly of *d* character. This is unlike the case for Ag$_2$, where the lowest optical excitation involves primarily (with 95% weight) the HOMO/LUMO pair of *s*/*sp* character, and *d* electrons start to participate in the absorption spectrum mainly above 6 eV. The analog of this *s* $\rightarrow sp$ transition in Ag$_2$ is the next allowed transition in Au$_2$ at 2.70 eV (associated with the experimental $X \rightarrow B$ line). This transition involves with 96% weight the HOMO-2/LUMO pair of the largest *s* character (HOMO-2 has ~85% *s* and 15% *d* characters). These first two allowed transitions in Au$_2$ are the only ones which can be mainly associated with a single *vc* pair in the corresponding eigenvectors. The rest of the transitions, as shown in Fig. 7, are linear combinations of at least two main *vc* pairs. For example, the transition at 5.49 eV (associated with the $X \rightarrow D$ line) is a combination of HOMO-2/LUMO+1 with 58% weight and HOMO-4/LUMO+1 with 41%.

A similar analysis of the orbital character of the optical excitations in Au$_{20}$ reveals the importance of *d* and *p* electrons even for low-energy excitations. As shown in Fig. 8, the lowest peak at 1.86 eV associated with the face-centered atoms is primarily a HOMO-1 (87% *s* and 10% *p* characters) to LUMO transition. However, the next significant peaks at 2.777 eV and 2.785 (associated with edge atoms) are linear
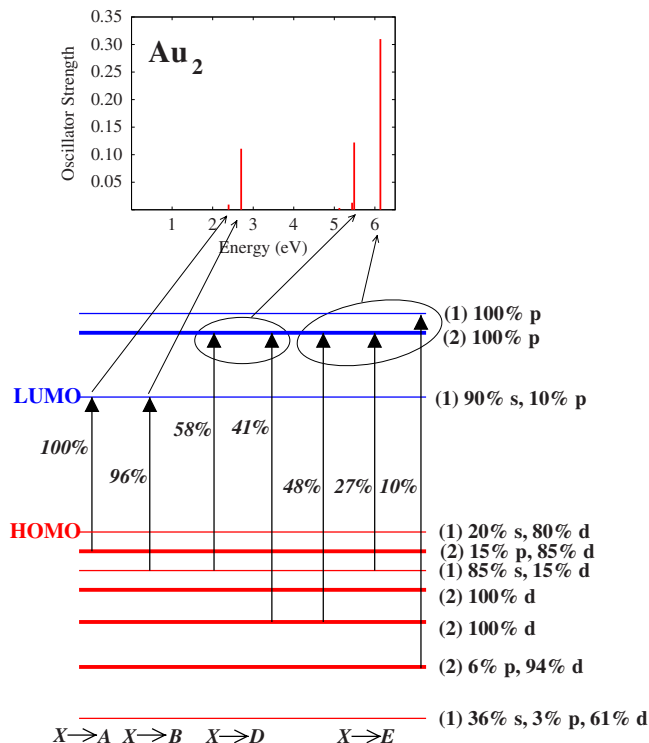
FIG. 7. (Color online) The Kohn-Sham energy levels (within LDA) of Au_2 that are involved in the excitations at 2.39, 2.70, 5.49, and 6.14 eV associated with the experimental $X \rightarrow A$, $X \rightarrow B$, $X \rightarrow D$, and $X \rightarrow E$ lines, respectively. The degeneracies (in parentheses) and the angular characters of the occupied and unoccupied orbitals involved in the transitions are given next to the energy levels. The weights (in %) of the vc orbital pairs in the eigenvectors of the transitions are also shown (see the text for details).
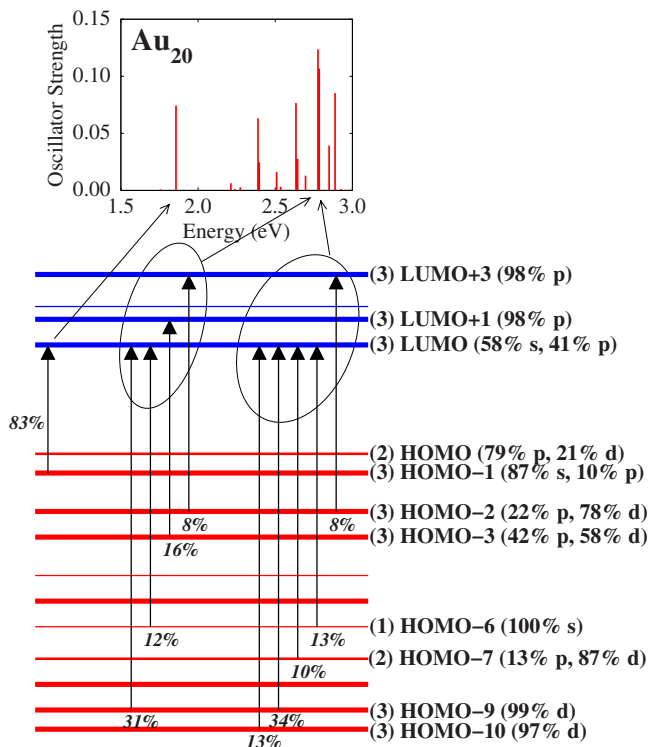

FIG. 8. (Color online) The Kohn-Sham energy levels (within LDA) of Au_{20} that are involved in the excitations at 1.86, 2.777, and 2.785 eV. The degeneracies (in parentheses) and the angular characters of the occupied and unoccupied orbitals involved in the transitions are given next to the energy levels. The weights (in %) of the vc orbital pairs in the eigenvectors of the transitions are also shown (see the text for details).

combinations of several vc pairs, in which the occupied orbitals have a significant amount of p and d characters. The peaks associated with the four vertex atoms (especially at 3.48 and 3.74 eV), not shown in Fig. 8, are primarily linear combination of vc pairs involving occupied orbitals of almost purely d character.

In order to quantify the contribution of d electrons to the optical spectra, we calculated the percentage of the d character in the transitions following the same method, as described in Ref. 91. We define the percent of the integrated d electron contributions over an energy range with a cutoff value of E_c as

$$\%d = \frac{\sum\limits_{i,\Omega_i < E_c} f_i \sum\limits_{vc} |F_i^{vc}|^2 |\langle d | \phi_v \rangle|^2}{\sum\limits_{i,\Omega_i < E_c} f_i} \times 100, \qquad (2)$$

where $\langle d | \phi_v \rangle$ is the $l = 2$ component of the occupied orbital ϕ_v. The degree of the integrated d character of the optical excitations for Au_n clusters calculated in this fashion is shown as a function of size for the cutoff energies of $E_c = 4$, 6, and 9 eV in Fig. 9. Also shown are the same results for Ag_n ($n \leq 8$). In the common size range, Au_n clusters have a significantly higher d-electron contribution to the optical ex-

citations no matter what the cutoff energy is. At $E_c = 9$ eV, the average integrated d-electron contribution to optical excitations for Au_n ($n \leq 8$) is above 60%, while it is about 15% for Ag_n clusters of the same size range. For small Au_n ($n \leq 5$), we observe that the d character increases significantly upon increasing the cutoff energy, which indicates that low-energy excitations in these clusters have considerable sp character. For larger Au_n clusters, d electrons contribute significantly to even low-energy absorption spectra. A similar
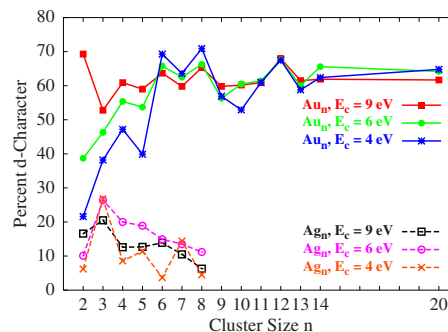

FIG. 9. (Color online) The percentage of the d character in the transitions calculated according to Eq. (2) for Au_n (solid lines) as a function of n at cutoff energies $E_c = 4$, 6, and 9 eV. Also shown are the same results for Ag_n (dashed lines).

trend is likely to be the case for larger Ag_n clusters, as our recent study[92] on Ag_{11} shows that the integrated d-electron contribution to optical excitations rapidly rises above $\sim E_c = 3$ eV, reaching values as high as 60% at $E_c = 6$ eV.

IV. SUMMARY

We presented results on and analyses of the static dipole polarizabilities and optical absorption spectra of the lowest energy structures of Au_n clusters, $n = 2 - 14$ and 20, obtained from first principles calculations within static and time-dependent DFTs. The static polarizabilities exhibit even-odd oscillations up to $n = 13$, after which they decrease noticeably due to the shape transition from two- to three-dimensional structures. This transition also manifests itself in the integrated oscillator strengths of the low-energy optical transitions. The TDLDA results for optical spectra are generally in good accord with available experimental data. The optical properties of Ag_n and Au_n clusters show significant differences. First, the enhanced screening of the s electrons by the d electrons gives rise to more quenched oscillator strengths (by $\sim 40\%$) in Au_n compared to Ag_n. Second, the d electrons are more directly involved in the low-energy optical excitations of Au_n clusters (even below 3 eV) in comparison to those of Ag_n. On average, the direct contribution of the d electrons in Au_n for excitations below 9 eV is in excess of 60%, which is a factor of $\sim 2-4$ larger than that in Ag_n. These stronger effects of the d electrons in the optical properties of Au_n clusters as compared to Ag_n clusters are explained by the larger degree of proximity of the s and d levels in the Au atom as compared to the Ag atom, which gives rise to stronger s-(p)-d hybridization in the molecular orbitals of Au_n.

*Present address: Physics Department, University of Wisconsin-Madison, Madison, Wisconsin, 53706, USA.

†The Chemistry Division became the Chemical Sciences and Engineering Division on 1 October 2007.

[1] P. Schwerdtfeger, Angew. Chem., Int. Ed. **42**, 1892 (2003).

[2] P. Pyykkö, Angew. Chem., Int. Ed. **43**, 4412 (2004); Inorg. Chim. Acta **358**, 4113 (2005).

[3] L. D. Socaciu, J. Hagen, T. M. Bernhardt, L. Wöste, U. Heiz, H. Häkkinen, and U. Landman, J. Am. Chem. Soc. **123**, 10437 (2003).

[4] B. Yoon, H. Häkkinen, U. Landman, A. S. Wörz, J.-M. Antonietti, S. Abbet, K. Judai, and U. Heiz, Science **307**, 403 (2005).

[5] S. Lee, C. Y. Fan, T. P. Wu, and S. L. Anderson, J. Chem. Phys. **123**, 124710 (2005).

[6] M. Haruta, Catal. Today **36**, 153 (1997).

[7] M. Valden, X. Lai, and D. W. Goodman, Science **281**, 1647 (1998).

[8] R. Meyer, C. Lemire, Sh. K. Shaikhutdinov, and H.-J. Freund, Gold Bull. **37**, 72 (2004).

[9] O. D. Häberlen, S.-C. Chung, M. Stener, and N. Rösch, J. Chem. Phys. **106**, 5189 (1997).

[10] G. Bravo-Pérez, I. L. Garzón, and O. Novaro, J. Mol. Struct.: THEOCHEM **493**, 225 (1999).

[11] H. Grönbeck and W. Andreoni, Chem. Phys. **262**, 1 (2000).

[12] R. Wesendrup, T. Hunt, and P. Schwerdtfeger, J. Chem. Phys. **112**, 9356 (2000).

[13] H. Häkkinen and U. Landman, Phys. Rev. B **62**, R2287 (2000).

[14] R. Mitrić, M. Hartmann, B. Stanca, V. Bonačić-Koutecký, and P. Fantucci, J. Phys. Chem. A **105**, 8892 (2001).

[15] H. Häkkinen, M. Moseler, and U. Landman, Phys. Rev. Lett. **89**, 033401 (2002).

[16] J. Wang, G. Wang, and J. Zhao, Phys. Rev. B **66**, 035418 (2002).

[17] V. Bonačić-Koutecký, J. Burda, R. Mitrić, and M. Ge, J. Chem. Phys. **117**, 3120 (2002).

[18] F. Furche, R. Ahlrichs, P. Weis, C. Jacob, S. Gilb, T. Bierweiler, and M. Kappes, J. Chem. Phys. **117**, 6982 (2002).

[19] S. Gilb, P. Weiss, F. Furche, R. Ahlrichs, and M. M. Kappes, J. Chem. Phys. **116**, 4094 (2002).

[20] H. Häkkinen, B. Yoon, U. Landman, X. Li, H.-J. Zhai, and L.-S. Wang, J. Phys. Chem. A **107**, 6168 (2003).

[21] R. Mitrić, C. Bürgel, J. Burda, V. Bonačić-Koutecký, and P. Fantucci, Eur. Phys. J. D **24**, 41 (2003).

[22] H. M. Lee, M. Ge, B. R. Sahu, P. Tarakeshwar, and K. S. Kim, J. Phys. Chem. B **107**, 9994 (2003).

[23] E. M. Fernández, J. M. Soler, I. L. Garzón, and L. C. Balbás, Phys. Rev. B **70**, 165403 (2004).

[24] L. Xiao and L. Wang, Chem. Phys. Lett. **392**, 452 (2004).

[25] B. Soulé de Bas, M. J. Ford, and M. B. Cortie, J. Mol. Struct.: THEOCHEM **686**, 193 (2004).

[26] F. Remacle and E. S. Kryachko, J. Chem. Phys. **122**, 044304 (2005).

[27] R. M. Olson, S. Varganov, M. S. Gordon, H. Metiu, S. Chretien, P. Piecuch, K. Kowalski, S. A. Kucharski, and M. Musial, J. Am. Chem. Soc. **127**, 1049 (2005).

[28] A. V. Walker, J. Chem. Phys. **122**, 094310 (2005).

[29] W. Fa, C. Luo, and J. Dong, Phys. Rev. B **72**, 205428 (2005).

[30] P. K. Jain, Struct. Chem. **16**, 421 (2005).

[31] Y.-K. Han, J. Chem. Phys. **124**, 024316 (2006).

[32] W. Fa and J. Dong, Appl. Phys. Lett. **89**, 013117 (2006).

[33] L. Xiao, B. Tollberg, X. Hu, and L. Wang, J. Chem. Phys. **124**, 114309 (2006).

[34] C. Majumder and S. K. Kulshreshtha, Phys. Rev. B **73**, 155427

(2006).

[35] E. M. Fernández, J. M. Soler, and L. C. Balbás, Phys. Rev. B **73**, 235433 (2006).

[36] S. Bulusu and X. C. Zeng, J. Chem. Phys. **125**, 154303 (2006).

[37] X. Xing, B. Yoon, U. Landman, and J. H. Parks, Phys. Rev. B **74**, 165423 (2006).

[38] X.-B. Li, H.-Y. Wang, X.-D. Yang, Z.-H. Zhu, J. Chem. Phys. **126**, 084505 (2007).

[39] Y. Dong and M. Springborg, Eur. Phys. J. D **43**, 15 (2007).

[40] L. M. Molina and J. A. Alonso, J. Phys. Chem. C **111**, 6668 (2007).

[41] B. Yoon, P. Koskinen, B. Huber, O. Kostko, B. von Issendorff, H. Häkkinen, M. Moseler, and U. Landman, ChemPhysChem **8**, 157 (2007).

[42] I. L. Garzón, K. Michaelian, M. R. Beltr'an, A. Posada-Amarillas, P. Ordejón, E. Artacho, D. Sánchez-Portal, and J. M. Soler, Phys. Rev. Lett. **81**, 1600 (1998).

[43] J. P. K. Doye and D. J. Wales, New J. Chem. **22**, 733 (1998).

[44] K. Michaelian, N. Rendon, and I. L. Garzón, Phys. Rev. B **60**, 2000 (1999).

[45] T. X. Li, S. Y. Yin, Y. L. Ji, B. L. Wang, G. H. Wang, and J. Zhao, Phys. Lett. A **267**, 403 (2000).

[46] J. M. Soler, I. L. Garzón, and J. D. Joannopoulos, Solid State Commun. **117**, 621 (2001).

[47] A. Lechtken, D. Schooss, J. R. Stairs, M. N. Blom, F. Furche, N. Morgner, O. Kostko, B. von Issendorf, and M. M. Kappes, Angew. Chem., Int. Ed. **46**, 2944 (2007).

[48] X. Gu, S. Bulusu, X. Li, X. C. Zeng, J. Li, X. G. Gong, and L.-S. Wang, J. Phys. Chem. **111**, 8228 (2007).

[49] J. Li, X. Li, H.-J. Zhai, and L.-S. Wang, Science **299**, 864 (2003).

[50] J. Wang, G. Wang, J. Zhao, Chem. Phys. Lett. **380**, 716 (2003).

[51] R. B. King, Z. Chen, and P. v. R. Schleyer, Inorg. Chem. **43**, 4564 (2004).

[52] E. Aprá, R. Ferrando, and A. Fortunelli, Phys. Rev. B **73**, 205414 (2006).

[53] M. P. Johansson, D. Sundholm, and J. Vaara, Angew. Chem., Int. Ed. **43**, 2678 (2004).

[54] J. Wang, J. Jellinek, J. Zhao, Z. Chen, R. B. King, P. v. R. Schleyer, J. Phys. Chem. A **109**, 9265 (2005).

[55] D. Tian, J. Zhao, B. Wang, and R. B. King, J. Phys. Chem. A **111**, 411 (2007).

[56] Y. Gao and X. C. Zeng, J. Am. Chem. Soc. **127**, 3698 (2005).

[57] X. Gu, M. Ji, S. H. Wei, and X. G. Gong, Phys. Rev. B **70**, 205401 (2004).

[58] S. Bulusu, X. Li, L.-S. Wang, and X. C. Zeng, Proc. Natl. Acad. Sci. U.S.A. **103**, 8326 (2006).

[59] H. Häkkinen, M. Moseler, O. Kostko, N. Morgner, M. A. Hoffmann, and B. v. Issendorff, Phys. Rev. Lett. **93**, 093401 (2004).

[60] P. Schwerdtfeger, Heteroat. Chem. **13**, 578 (2002).

[61] L. L. Ames and R. F. Barrow, Trans. Faraday Soc. **63**, 39 (1967).

[62] D. M. Gruen, S. L. Gaudiosi, R. L. McBeth, and J. L. Lerner, J. Chem. Phys. **60**, 89 (1974).

[63] W. E. Klotzbücher and G. A. Ozin, Inorg. Chem. **19**, 3767 (1980).

[64] R. Marcus and N. Schwentner, in *Physics and Chemistry of Small Clusters*, edited by P. Jena, B. K. Rao, and S. N. Khanna (Plenum, New York, 1987), p. 611.

[65] G. A. Bishea and M. D. Morse, J. Chem. Phys. **95**, 5646 (1991).

[66] G. A. Bishea and M. D. Morse, J. Chem. Phys. **95**, 8779 (1991).

[67] W. Harbich, S. Fedrigo, J. Buttet, and D. M. Lindsay, J. Chem. Phys. **96**, 8104 (1992).

[68] S. Fedrigo, W. Harbich, and J. Buttet, J. Chem. Phys. **99**, 5712 (1993).

[69] H. Handschuh, G. Gantef̈or, P. S. Bechthold, and W. Ederhardt, J. Chem. Phys. **100**, 7093 (1994).

[70] B. A. Collings, K. Athanassenas, D. Lacombe, D. M. Rayner, and P. A. Hackett, J. Chem. Phys. **101**, 3506 (1994).

[71] A. Schweizer, J. M. Weber, S. Gilb, H. Schneider, D. Schooss, and M. M. Kappes, J. Chem. Phys. **119**, 3699 (2003).

[72] S. Gilb, K. Jacobsen, D. Schooss, F. Furche, R. Ahlrichs, and M. M. Kappes, J. Chem. Phys. **121**, 4619 (2004).

[73] J. Zheng, C. Zhang, and R. M. Dickson, Phys. Rev. Lett. **93**, 077402 (2004); J. Zheng, P. R. Nicovich, and R. M. Dickson, Annu. Rev. Phys. Chem. **58**, 409 (2007).

[74] P. Neogrády, V. Kellö, M. Urban, and A. J. Sadlej, Int. J. Quantum Chem. **63**, 557 (1997).

[75] T. Saue and H. J. A. Jensen, J. Chem. Phys. **118**, 522 (2003).

[76] J. Zhao, J. Yang, and J. G. Hou, Phys. Rev. B **67**, 085404 (2003).

[77] B. O. Roos, R. Lindh, P. Malmqvist, V. Veryazov, and P. Widmark, J. Phys. Chem. A **109**, 6575 (2005).

[78] F. Wang and W. Liu, Chem. Phys. **311**, 63 (2005).

[79] J. Wang, M. Yang, J. Jellinek, and G. Wang, Phys. Rev. A **74**, 023202 (2006).

[80] J. Lermé, B. Palpant, B. Prével, E. Cottancin, M. Pellarin, M. Treilleux, J. L. Vialle, A. Perez, and M. Broyer, Eur. Phys. J. D **4**, 95 (1998).

[81] M. A. Omary, M. A. Rawashdeh-Omary, C. C. Chusuei, J. P. Fackler, Jr., and P. S. Bagus, J. Chem. Phys. **114**, 10695 (2001).

[82] X. Wang, X. Wan, H. Zhou, S. Takami, M. Kubo, and A. Miyamoto, J. Mol. Struct.: THEOCHEM **579**, 221 (2002).

[83] I. Itkin and A. Zaitsevskii, Chem. Phys. Lett. **374**, 143 (2003).

[84] R. Guo, K. Balasubramanian, X. Wang, and L. Andrews, J. Chem. Phys. **117**, 1614 (2002).

[85] K. Wu, J. Li, and C. Lin, Chem. Phys. Lett. **388**, 353 (2004).

[86] R.-H. Xie, G. W. Bryant, J. Zhao, T. Kar, and V. H. Smith, Jr., Phys. Rev. B **71**, 125422 (2005).

[87] C. M. Aikens and G. C. Schatz, J. Phys. Chem. A **110**, 13317 (2006).

[88] F. Wang and T. Ziegler, J. Chem. Phys. **122**, 204103 (2005).

[89] W. Fa, J. Zhou, C. Luo, and J. Dong, Phys. Rev. B **73**, 085405 (2006).

[90] J. L. Rao, G. K. Chaitanya, S. Basavaraja, K. Bhanuprakash, and A. Venkataramana, J. Mol. Struct.: THEOCHEM **803**, 89 (2007).

[91] J. C. Idrobo, S. Öğüt, and J. Jellinek, Phys. Rev. B **72**, 085445 (2005).

[92] J. C. Idrobo, S. Öğüt, K. Nemeth, J. Jellinek, and R. Ferrando, Phys. Rev. B **75**, 233411 (2007).

[93] S. Öğüt, J. C. Idrobo, J. Wang, and J. Jellinek, J. Cluster Sci. **17**, 609 (2006).

[94] J. P. Perdew, K. Burke, and M. Ernzerhof, Phys. Rev. Lett. **77**, 3865 (1996).

[95] B. Delley, Phys. Rev. B **66**, 155125 (2002).

[96] J. R. Chelikowsky, N. Troullier, and Y. Saad, Phys. Rev. Lett. **72**, 1240 (1994); J. R. Chelikowsky, N. Troullier, K. Wu, and Y. Saad, Phys. Rev. B **50**, 11355 (1994).

[97] N. Troullier and J. L. Martins, Phys. Rev. B **43**, 1993 (1991).

[98] L. Kleinman and D. M. Bylander, Phys. Rev. Lett. **48**, 1425 (1982).

[99] D. M. Ceperley and B. J. Alder, Phys. Rev. Lett. **45**, 566 (1980).

[100] I. Vasiliev, S. Öğüt, and J. R. Chelikowsky, Phys. Rev. Lett. **78**, 4805 (1997).

[101] H. A. Kurtz, J. J. P. Stewart, and K. M. Dieter, J. Comput. Chem. **96**, 231 (1990); A. A. Quong and M. R. Pederson, Phys. Rev. B **46**, 12906 (1992); I. Moullet, J. L. Martins, F. Reuse, and J. Buttet, *ibid.* **42**, 11598 (1990); D. Porezag and M. R. Pederson, *ibid.* **54**, 7830 (1996).

[102] M. E. Casida, in *Recent Advances in Density-Functional Methods*, edited by D. P. Chong (World Scientific, Singapore, 1995), Pt. I, p. 155; *Recent Developments and Applications of Modern Density Functional Theory*, edited by J. M. Seminario (Elsevier, Amsterdam, 1996), p. 391.

[103] I. Vasiliev, S. Öğüt, and J. R. Chelikowsky, Phys. Rev. Lett. **82**, 1919 (1999); Phys. Rev. B **65**, 115416 (2002).

[104] K. A. Jackson, M. Yang, I. Chaudhuri, and T. Frauenheim, Phys. Rev. A **71**, 033205 (2005).

[105] J.-M. Antonietti, M. Michalski, U. Heiz, H. Jones, K. H. Lim, N. Rösch, A. DelVitto, and G. Pacchioni, Phys. Rev. Lett. **94**, 213402 (2005).

[106] M. Walter and H. Häkkinen, Phys. Rev. B **72**, 205440 (2005).

[107] J. C. Ehrhardt and S. P. Davis, J. Opt. Soc. Am. **61**, 1342 (1971); D. C. Morton, Astrophys. J., Suppl. Ser. **130**, 403 (2000).

[108] J. C. Idrobo, M. Yang, K. A. Jackson, and S. Öğüt, Phys. Rev. B **74**, 153410 (2006).